Biosensors and Bioelectronics 130 (2019) 230–235

Contents lists available at ScienceDirect

Biosensors and Bioelectronics

journal homepage: www.elsevier.com/locate/bios

Design and construction of Z-scheme Bi_2S_3/nitrogen-doped graphene quantum dots: Boosted photoelectric conversion efficiency for high-performance photoelectrochemical aptasensing of sulfadimethoxine

Fuheng You[a], Mingyue Zhu[a], Lijun Ding[a], Yuhuan Xu[a], Kun Wang[a,b,*]

[a] Key Laboratory of Modern Agriculture Equipment and Technology, School of Chemistry and Chemical Engineering, Jiangsu University, Zhenjiang 212013, PR China
[b] Key Laboratory of Sensor Analysis of Tumor Marker, Ministry of Education, College of Chemistry and Molecular Engineering, Qingdao University of Science and Technology, Qingdao 266042, PR China

ARTICLE INFO

Keywords:
Z-scheme
Bismuth sulfide
Nitrogen-doped graphene quantum dot
Visible light
Photoelectrochemical aptasensor

ABSTRACT

Rational design and fabrication of Z-scheme visible-light-driven photoactive materials have drawn much attention owing to their great potential in handling environment and energy crisis. In this work, Z-scheme Bi_2S_3/nitrogen-doped graphene quantum dots (NGQDs) with superior photoelectric conversion efficiency were designed and fabricated, which demonstrated enhanced photoactivity compared with Bi_2S_3 owing to the improved separation efficiency of photogenerated electron and hole pairs. The emphasis was put on designing Z-scheme Bi_2S_3/NGQDs, and then the mechanism of Z-scheme charge transfer mode was verified by the electron spin resonance (ESR) technique. On this basis, the proposed sensor exhibited a wide linear range of 0.1–120 nM and a detection limit of 0.03 nM (S/N = 3) for SDM, with high sensitivity (0.075 μA nM^{-1}), good selectivity and stability. Moreover, the proposed PEC aptasensor using Bi_2S_3/NGQDs as the photoelectrode achieved sensitive and selective determination of sulfadimethoxine in milk samples. This work could provide some ideas for designing other Z-scheme photoactive species and insights into the charge transfer mechanism of Z-scheme. Furthermore, the promising applicability of PEC aptasensor using photoactive species could be extended to other accurate monitoring for contaminants.

1. Introduction

Visible-light-driven photoactive species are identified as promising and ideal candidates for extensive photochemical applications in resolving the environment and energy crisis due to its higher utilization efficiency to the solar light (Chen et al., 2010; Kubacka et al., 2016; Hong et al., 2016). To achieve these demanding goals, various Z-scheme type systems have been investigated based on semiconductors possessing band structures with a staggered alignment and different band gaps (Yang et al., 2013; Li et al., 2015). These systems utilize broadband light adsorption, efficient separation and transport of photogenerated charges, as well as preserve sufficient band-edge potential (Bai et al., 2015; Yuan et al., 2017). Compared with the typical heterojunction system, the construction of Z-scheme type systems can reduce the recombination of photogenerated electron–hole pairs and maintain excellent redox ability (Zhou et al., 2014). However, the majority of the fabricated Z-scheme systems always included noble metal (Ag, Ru) (Wang et al., 2011; Sasaki et al., 2013) or redox pair (IO_3^-/I^-, Fe^{3+}/Fe^{2+}) (Maeda et al., 2013), leading to much difficulty in practical applications. Thence, it is significant to design a new Z-scheme system on basis of visible-light-responsive photoactive materials.

Bismuth sulfide (Bi_2S_3), a semiconductor with a narrow band gap (E_g) of 1.3 eV, has attracted much attention in photochemical applications and PEC sensors due to its better photo-electron conversion efficiency (Liu et al., 2015, 2017a, 2017b; Gao et al., 2016). Recently, Wang's group constructed a CdTe-Bi_2S_3 heterojunction for fabricating photoelectrochemical (PEC) biointerface, which exhibited obvious change of photocurrent responses during the detecting process (Liu et al., 2017a, 2017b). Nevertheless, the focus is still developing more efficient systems to obtain improved separation and transfer of photogenerated charges. Fortunately, the formation of Z-scheme type heterostructure by integrating two semiconductors which have proper band energies can improve the separation efficiency of photogenerated electron-hole pairs, and thus enhance the photoactivity of fabricated systems (Wetchakun et al., 2012). Nitrogen-doped graphene quantum dots (NGQDs) can serve as an ideal electron mediate due to its

* Corresponding author.
E-mail address: wangkun@ujs.edu.cn (K. Wang).

https://doi.org/10.1016/j.bios.2019.01.058
Received 1 November 2018; Received in revised form 19 January 2019; Accepted 22 January 2019
Available online 05 February 2019
0956-5663/

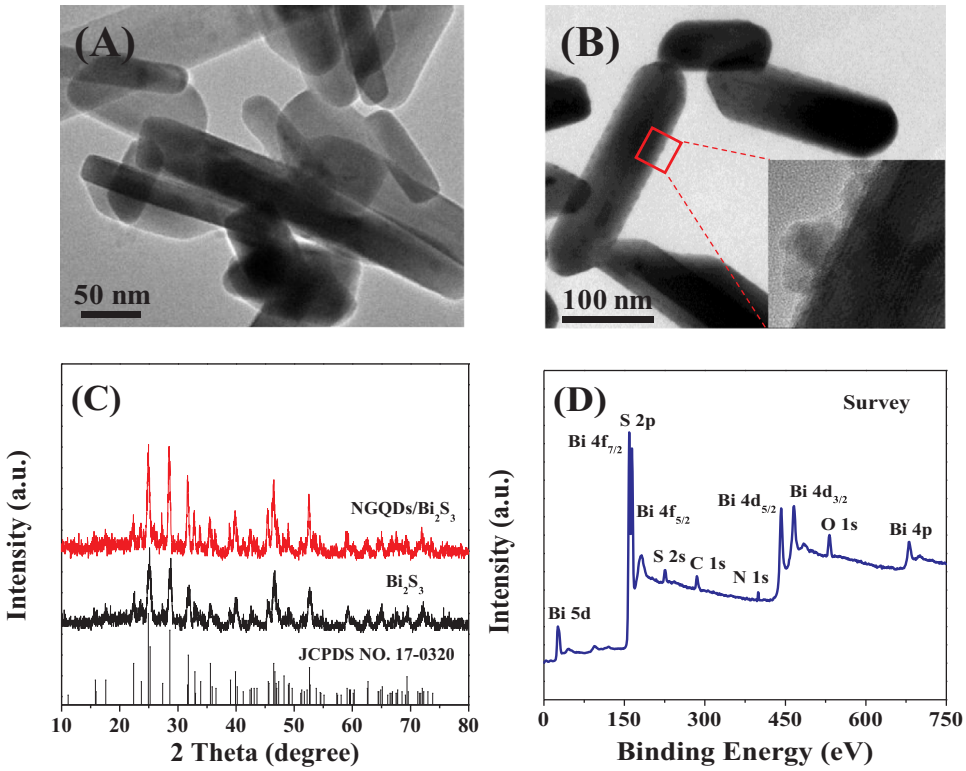

Fig. 1. TEM images of (A) Bi_2S_3 and (B) Bi_2S_3/NGQDs and (C) XRD patterns of Bi_2S_3 and Bi_2S_3/NGQDs and (D) XPS survey spectrum of Bi_2S_3/NGQDs.

superiorities in conductivity, biocompatibility, and photochemical properties (Li et al., 2012; Zhu et al., 2017; Yan et al., 2016). In this work, the PEC activity was dramatically enhanced by the Bi_2S_3/NGQDs formation with Z-scheme structure, which was benefit for improving the sensitivity of the photoelectrochemical sensor. PEC aptasensor, coupling the advantages of PEC technique and aptamer, has been regarded as an effective detection method in bioanalysis. This method has significant merits, such as high sensitivity, low background, and specific selectivity (Zhao et al., 2014, 2016). Two important elements should be included in PEC aptasensor: 1) the PEC active materials transferring photoirradiation into electrical signal, 2) biological recognition aptamer identifying specific target molecules for bioanalysis (Zhao et al., 2015). To achieve these two requirements, photoactive species with superior photoelectric conversion efficiency and targeted biomolecules are required.

Sulfadimethoxine (SDM) has been extensively used in veterinary treatment of coccidiosis and other bacterial infections (Song et al., 2012), however, an early study suggests that SDM at low concentration also has toxic effects on the target organisms and even the whole ecosystem (Białk-Bielińska et al., 2012). Thus, the sensitive detection of SDM is needed even at low concentrations. Herein, an efficient PEC aptasensor for sensitive and selective detection of SDM was established on the basis of Z-scheme type Bi_2S_3/NGQDs as the photoactive reagent. The proposed PEC aptasensor exhibited several merits including wide linear range, low detection limit, good selectivity and satisfactory recoveries when it was used to quantify SDM in real milk samples. Moreover, the mechanism for the enhanced PEC activity of Z-scheme Bi_2S_3/NGQDs was also studied.

2. Experimental section

2.1. Preparation of Bi_2S_3/NGQDs

Bi_2S_3 and NGQDs were obtained according to previous literatures with modification (Okoth et al., 2016; Yin et al., 2016). 1.82 g Bi $(NO_3)_3{\cdot}5H_2O$ was dissolved in 25 mL ethylene glycol, which was stirred for 30 min to obtain solution A. 1.35 g $Na_2S{\cdot}9H_2O$ was dissolved in 30 mL ultrapure water to obtain solution B. Then, solution B was added drop-wise into solution A, coming into being a large mass of black suspension. Meanwhile, 1.35 g urea was also dissolved in 20 mL ultrapure water and then put into the above suspension. Subsequently, NGQDs with a certain amount was also added dropwise into the suspension, which was further stirred for 30 min. The resulting mixture was transferred into a Teflon lined stainless steel autoclave, sealed and maintained at 160 °C for 12 h, and the product was centrifuged and washed with ultrapure water and alcohol for several times. The final products were then dried to obtain the Bi_2S_3/NGQDs powder. In the same way, Bi_2S_3 were synthesized without adding NGQDs.

2.2. Construction of PEC aptasensing interface

Prior to fabrication, ITO electrodes were treated with NaOH (0.5 M) solution and sonicated in ultrapure water and alcohol. Then, 20 μL of Bi_2S_3/NGQDs dispersion with a concentration of 2 mg mL^{-1} was casted onto ITO and then dried at room temperature. Subsequently, 20 μL of 0.05% chitosan (CHIT) solution as the fixing agent was decorated on the ITO electrode. After then, served as a cross linker for the amine-functionalized aptamer, 20 μL of 0.05% glutaraldehyde (GA) was dropped on and left at room temperature for 1 h. Next, 20 μL of amine-functionalized SDM aptamer (2.5 μM) was immobilized on the CHIT/Bi_2S_3/NGQDs/ITO electrode surface and incubated at 4 °C for 12 h. It is mentioned that NH_2 group in the aptamer is covalently attached to NH_2 group of the immobilized CHIT on the ITO electrode using glutaraldehyde (GA) as crosslinking agent (Khezrian et al., 2013). The obtained aptamer/GA/CHIT/Bi_2S_3/NGQDs/ITO electrode was rinsed thoroughly with PBS (pH 7.0) to remove unabsorbed aptamers. The amount of the aptamer on the modified electrode surface were estimated by a One Drop™ OD-1000 spectrophotometer (Thermo Fisher Scientific, Waltham, USA) at 260 nm, and the amount of aptamer combined on the electrode surface is 0.02712 OD. Then, the interface

was covered with 10 μL (1 mM) bull serum albumin (BSA) and then was put in room temperature for 1 h to block nonspecific active sites, followed by rinsing with ethanol and ultrapure water, respectively (Zhao et al., 2012). Finally, the PEC signals of the SDM-aptamer/GA/CHIT/Bi_2S_3/NGQDs/ITO were used for SDM detection.

3. Results and discussion

3.1. Characterization of the samples

TEM was investigated to obtain the detailed morphologies of Bi_2S_3 and Bi_2S_3/NGQDs. As shown in Fig. 1A, the surface of Bi_2S_3 was pretty smooth and clear to be seen. Moreover, Fig. 1B demonstrated the TEM image of Bi_2S_3/NGQDs, which illustrated that NGQDs was decorated on the Bi_2S_3 surface. Furthermore, it was obvious that Bi_2S_3/NGQDs surface became rougher than Bi_2S_3 (the inset of Fig. 1B).

The phases of Bi_2S_3 and Bi_2S_3/NGQDs were characterized by XRD. As shown in Fig. 1C, some main diffraction peaks around 25.02°, 28.51°, 31.79°, 35.66°, 46.64°, and 52.60° were detected for Bi_2S_3 (curve a) and Bi_2S_3/NGQDs (curve b), which were ascribed to the (130), (211), (301), (240), (431), and (351) planes of Bi_2S_3 (JCPDS NO. 17–0320) (Fang et al., 2011). However, no obvious diffraction peaks of NGQDs were heeded in Bi_2S_3/NGQDs owing to a little content and high dispersion that could not be resolved by XRD (Yin et al., 2016). Besides, no other diffraction peak was found in Bi_2S_3/NGQDs, which suggested the high-purity of as-prepared sample.

XPS analysis was employed to elucidate the chemical composition and electronic structure of Bi_2S_3/NGQDs. As shown in Fig. 1D, Bi_2S_3/NGQDs was composed by Bi, S, C, O and N elements. Fig. S1A revealed the high-resolution XPS spectra of Bi 4 f and S 2p, as shown, the Bi 4 $f_{7/2}$ and Bi 4 $f_{5/2}$ peaks at 158.4 and 163.8 eV, and the S 2p peak at 161.2 eV (Rauf et al., 2015). Furthermore, high-resolution XPS spectra of C1s (Fig. S1B) peaks at 284.6, 285.2, 286.6, 287.4, and 288.9 eV were ascribed to C–C, C–N, C–O, C=O, and O–C=O, respectively (Yin et al., 2016). In addition, the N 1s (Fig. S1C) spectrum illustrated four peaks around pyridine N, pyrrolic N, graphitic N, and N − H, respectively (Yin et al., 2016). All these characterizations above proved the Bi_2S_3/NGQDs were successfully synthesized.

3.2. PEC properties of the modified electrodes

So as to examine the PEC behavior of different electrodes, a comparative trial was investigated under visible light irradiation. As illustrated in Fig. 2A, the PEC responses of Bi_2S_3/ITO (curve a) and Bi_2S_3/NGQDs/ITO (curve b) were 5.8 and 12.0 μA, which was ascribed to the effective separation of photogenerated electron–hole pairs in Bi_2S_3/NGQDs. Furthermore, EIS characterization was employed to study the charge transfer processes (Jiang et al., 2015). As shown in Fig. 2B, Bi_2S_3/NGQDs/ITO (curve b) demonstrated a decreased diameter of the semicircle compared to Bi_2S_3/ITO (curve a), suggesting that the introduction of NGQDs modified Bi_2S_3 could accelerate the charge transfer process on the electrode surface. It's generally accepted that the recombination of photogenerated charges could enhance the PL emission signal (Xu et al., 2013), thus the PL technique was employed in this work. As demonstrated in Fig. S2, Bi_2S_3/NGQDs possessed a weaker peak than Bi_2S_3, which suggested the formation of Bi_2S_3/NGQDs could accelerate the separation of photogenerated electron–hole pairs (Jiang et al., 2012).

3.3. Fabrication of PEC aptasensor

A selective and sensitive PEC aptasensor was established with visible-light-driven Bi_2S_3/NGQDs photoactive species for SDM detection. Fig. 3A represents the photocurrent of aptasensor during the fabrication and detection process. For Bi_2S_3/NGQDs/ITO (curve a), a relative high photocurrent was obtained, suggesting the effective separation of photogenerated electron and holes. After CHIT molecules assembly, the photocurrent intensity demonstrated a little decrease (curve b). This revealed that CHIT molecules had no obvious effect on Bi_2S_3/NGQDs as photoactive materials. Furthermore, the photocurrent signal was found to be further decrease after immobilization of the aptamer (curve c). This could be explained that the steric hindrance from the aptamer prevented the transfer of electrons (Zang et al., 2014). However, the photocurrent response increased after formation of a complex between aptamer and SDM (curve d). This could be ascribed that SDM molecules captured by the aptamer was oxidized by the photogenerated holes.

To confirm the success of the fabricating process of the PEC aptasensor, EIS analysis was employed to investigate the interfacial charge transfer resistance (R_{ct}) (Jiang et al., 2016). As demonstrated in Fig. 3B, Bi_2S_3/NGQDs/ITO (curve a) and CHIT/Bi_2S_3/NGQDs/ITO (curve b) exhibited smaller R_{ct} due to their good conductivity. However, the value of R_{ct} increased dramatically after the aptamer modified on the electrode (curve c), which might be attributed that aptamer molecules with negative charges could induce the electrostatic repulsion between the electrode surface and redox species of $[Fe(CN)_6]^{3-/4-}$ (Li et al., 2014). After SDM incubation (curve d), the aptamer on the electrode had a specific reaction with SDM, and then, with the SDM oxidation process, more photogenerated holes were consumed and thus more electrons were transferred to the electrode, leading to the reduced R_{ct}. In view of PEC signals and EIS results, the PEC aptasensor was established successfully.

3.4. Optimization of conditions for PEC aptasensor

To fabricate a highly sensitive PEC aptasensor for SDM detection,

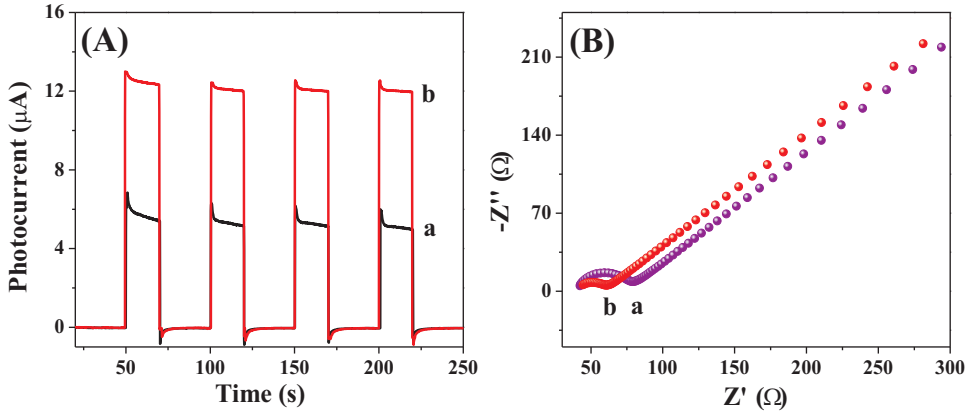

Fig. 2. (A) Photocurrent and (B) EIS responses of Bi_2S_3/ITO (a) and Bi_2S_3/NGQDs/ITO (b).

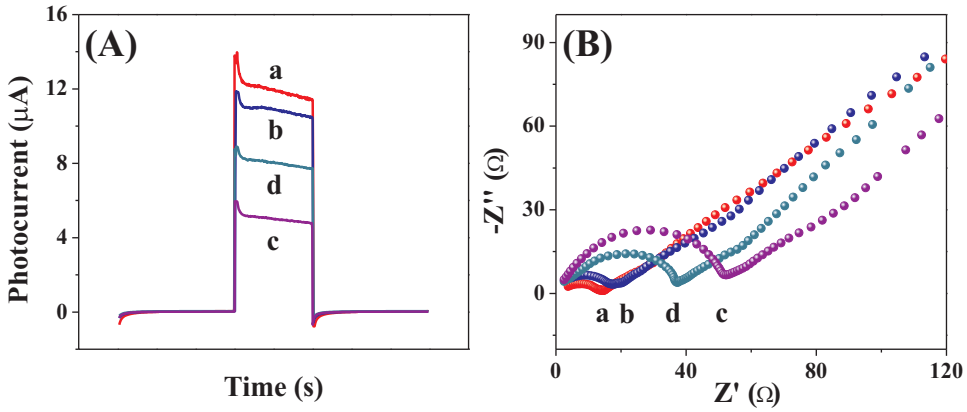

Fig. 3. (A) PEC and (B) EIS characterization of aptasensor fabrication process: Bi_2S_3/NGQDs/ITO (a), CHIT/Bi_2S_3/NGQDs/ITO (b), aptamer/CHIT/Bi_2S_3/ NGQDs/ITO (c), and 10 nM SDM interact with aptamer/CHIT/Bi_2S_3/NGQDs/ITO (d).

some experimental parameters involved the NGQDs content in Bi_2S_3/NGQDs, the aptamer concentration, and the incubation time of SDM with aptamer were optimized. Fig. S3 indicates the photocurrent signals increased initially and then declined with the content of NGQDs increased from 0.5 mL to 8.0 mL. This demonstrated that the appropriate doping of NGQDs could improve the PEC activity of Bi_2S_3/NGQDs (Yin et al., 2016), and Bi_2S_3/NGQDs (2.0 mL) with a maximum photocurrent signal was selected for establishing PEC aptasensor in this work. Fig. S4 displays that the photocurrent declined gradually and then keep invariable when the aptamer concentration from 0.5 to 3.0 μM, which was ascribed to the aptamer could prevent the electrons transfer. It is clear that 2.5 μM of aptamer concentration had reached a certain saturation point, thus, 2.5 μM was chosen as the optimal aptamer concentration.

3.5. Analytical performance of the PEC aptasensor

Under optimal conditions, the resulted PEC aptasensor toward SDM was established by recording the photocurrent signals. As illustrated in Fig. 4A, the photocurrent responses increased obviously with the concentration increased of SDM. Moreover, Fig. 4B demonstrated the relationship between the photocurrent response (I) and the concentration (c) of SDM. And a good linear relationship was determined from 0.1 to 120 nM. The detection limit was 0.03 nM (S/N = 3), which was lower than the reported results shown in Table S1.

3.6. Selectivity and stability of PEC aptasensor

To confirm the specificity of the fabricated PEC aptasensor, some representative interfering species were involved in the interference test. During this process, the variation of photocurrent intensity (ΔI) of 10 nM SDM, 100 nM Kanamycin, Tetracycline, Oxytetracycline, Streptomycin, and Chloramphenicol were recorded. As shown in Fig. 4C, dramatic photocurrent vary was received only in the existence of SDM, for comparison, no obvious change photocurrent was observed when the aptasensor toward other nontarget molecules, suggesting

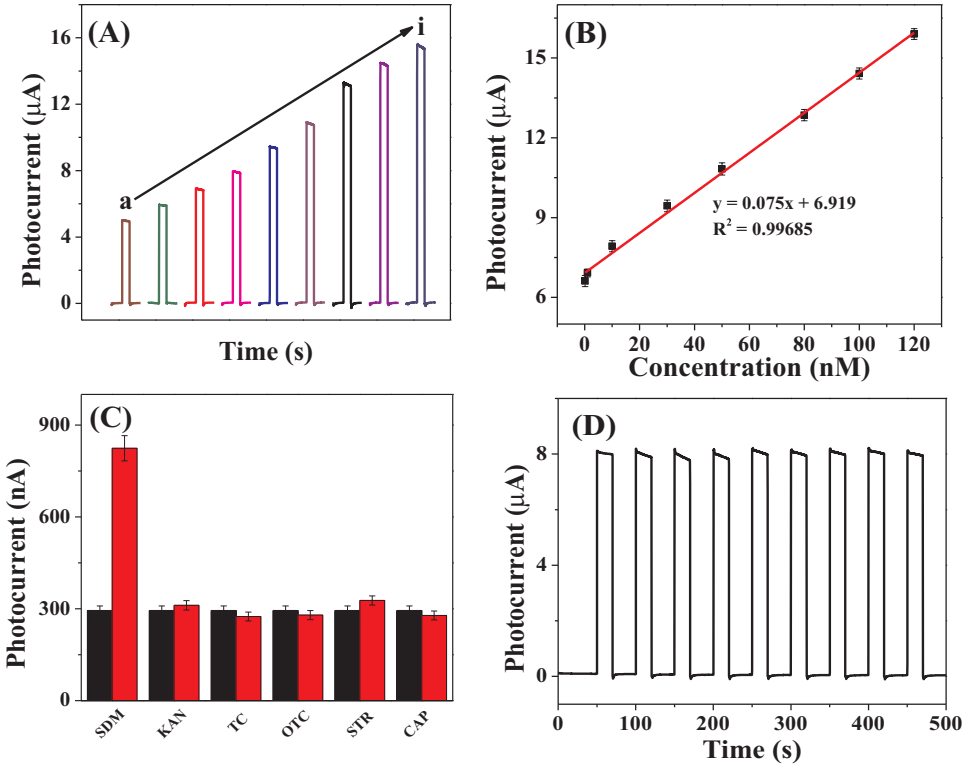

Fig. 4. (A) Photocurrent response of the PEC aptasensor at different concentrations of SDM: 0 (a), 0.1 (b), 1 (c), 10 (d), 30 (e), 50 (f), 80 (g), 100 (h), and 120 nM (i). (B) The corresponding linear calibration curve. (C) Selectivity of the SDM PEC aptasensor. (D) Stability test of SDM PEC aptasensor for SDM at the concentration of 10 nM.

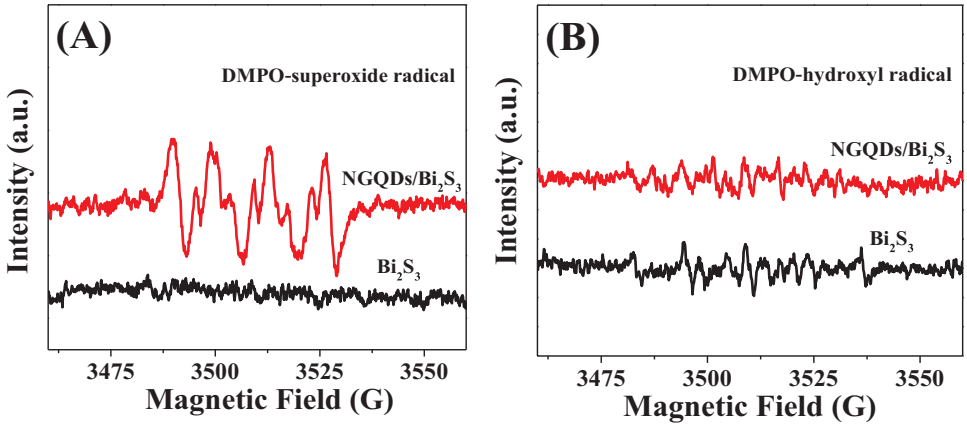

Fig. 5. DMPO spin-trapping ESR spectra in aqueous dispersion of Bi_2S_3 and Bi_2S_3/NGQDs for (A) DMPO-superoxide radical and (B) DMPO-hydroxyl radical irradiated for 120 s.

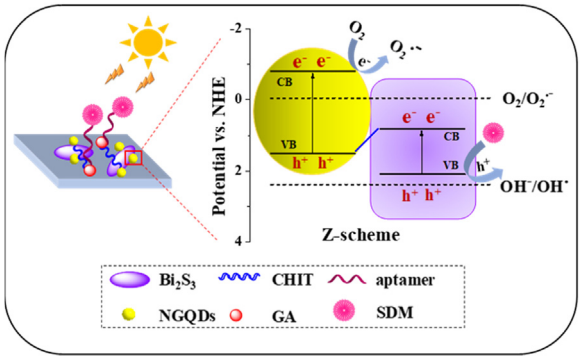

Fig. 6. Schematic illustration of PEC aptasensing of SDM based on Bi_2S_3/NGQDs.

good specificity of the established PEC aptasensor, which should be ascribed to the specific binding of SDM to the aptamer. Therefore, the proposed sensor can detect SDM in the presence of other interferences. In addition, the photocurrent signal was collected under nine on-off cycles to test the stability of the PEC aptasensor. Fig. 4D did not show noticeable variation, revealing the stable signal for photocurrent collection. Furthermore, the reproducibility was also examined by a relative standard deviation (RSD) through recording five independent electrodes, which were modified 10 nM SDM at the same conditions. Then RSD was calculated to be 5.6%, which demonstrated the acceptable reproducibility of the proposed PEC aptasensor.

3.7. Application in milk samples

The applicability of the established aptasensor was studied in real milk samples, which was purchased from the local supermarket and then treated according to the previous method. These milks were bought from a local supermarket and the brand is Yili. 2 mL of milk and 2 mL of PBS were mixed. And after magnetic stirring for 10 min, 7 mL of ethyl acetate was added, shook the mixed solution vigorously for 15 min and then centrifuged the solution at 5000 rpm for 15 min, took the supernatant. After that, added 7 mL of ethyl acetate and repeat the above steps. The ethyl acetate was then removed from the collected supernatant by a gentle nitrogen blow-down at 40 °C. After this process, the final precipitate was dissolved in PBS, 1, 10, and 30 nM (0.31, 3.1, and 9.3 $\mu g\,L^{-1}$) of sulfadimethoxine were added to the extracted milk sample (Song et al., 2012; Okoth et al., 2016). The results were listed in Table S2, the recoveries of the aptasensor were from 98.2% to 102.0% with a RSD value of 3.2 ~ 5.6%, which indicated the potential applicability of the fabricated aptasensor for SDM monitoring in milk samples.

3.8. Mechanism study

The energy levels of Bi_2S_3 determines the route of photogenerated charges transfer in the Bi_2S_3/NGQDs, thus, the conduction band (CB) and valence band (VB) levels of Bi_2S_3 are important and necessary in this system, which were calculated according to the following formula: (Liu et al., 2017a, 2017b)

$$E_{CB}(eV) = -\chi + 0.5E_g \quad (1)$$

$$E_{VB}(eV) = -\chi - 0.5E_g \quad (2)$$

Where χ and E_g are the electronegativity and band gap energy of Bi_2S_3. According to the literature, the χ value of Bi_2S_3 is estimated to be 5.95 eV (Zhang et al., 2012). The E_g value (1.28 eV) was obtained from the Tauc's plots of Bi_2S_3 (shown in Fig. S5) (Zhu et al., 2014). According to the formula above, the CB and VB values of Bi_2S_3 were 0.81 and 2.09 eV (vs NHE). We examined the energy levels of NGQDs using linear potential scans for determining the CBM and VBM energy levels (Yeh et al., 2014). As demonstrated in Fig. S6 and after calculation, CB and VB values of NGQDs were − 0.8 and 1.5 eV (vs NHE).

ESR technique was used to detect the presence of $O_2^{\bullet-}$ (superoxide radical) and $^{\bullet}OH$ (hydroxyl radical) in the Bi_2S_3 and Bi_2S_3/NGQDs under visible light irradiation. As shown in Fig. 5, neither $O_2^{\bullet-}$ nor $^{\bullet}OH$ could be observed in the ESR spectra of Bi_2S_3. While with the introduction of NGQDs, $O_2^{\bullet-}$ could be observed in Bi_2S_3/NGQDs, which was attributed to the fact that the photogenerated electrons of CB (− 0.8 eV) for NGQDs were negative enough to reduce O_2 to $O_2^{\bullet-}$ (–0.046 eV). Moreover, $^{\bullet}OH$ was not observed for the Bi_2S_3/NGQDs, due to the VB of Bi_2S_3 (− 2.09 eV) was not positive than redox potential of $^{\bullet}OH/OH^-$ (2.38 eV), hence the h^+ could not oxidize OH^- to $^{\bullet}OH$ (Xia et al., 2016). In accordance with the description above, a Z-scheme-type charge transfer in Bi_2S_3/NGQDs was presented. As illustrated in Fig. 6, both Bi_2S_3 and NGQDs are easily excited under visible-light irradiation and correspondingly, photoexcited electrons and holes are generated in CB and VB, respectively. The electrons in CB (0.8 eV) of Bi_2S_3 transfer to the VB of NGQDs, and then coincide with the holes in VB (1.5 eV) of NGQDs. This process resulted in leaving behind the holes in the VB of Bi_2S_3, which could directly oxidize SDM molecules.

4. Conclusions

In summary, a simple PEC aptasensor for sensitive and selective detection of SDM was established based on Z-scheme Bi_2S_3/NGQDs with superior photo-electric conversion efficiency. Bi_2S_3/NGQDs as the photoelectrode coupled efficient PEC technique with highly specific

aptamer resulted in good sensitivity and selectivity of the proposed aptasensor. Also, the mechanism for the enhanced photoactivity of Bi_2S_3/NGQDs was investigated. The proposed PEC aptasensor exhibited great merits including wide linear range, low detection limit, excellent selectivity and satisfactory recoveries when it was used to quantify SDM in real milk samples. The formation of such sensitized Z-scheme composites provides a feasible method to fabricate a universal biointerface for PEC analysis.

CRediT authorship contribution statement

Fuheng You: Investigation, Writing - original draft. **Mingyue Zhu:** Methodology, Supervision. **Lijun Ding:** Data curation. **Yuhuan Xu:** Formal analysis. **Kun Wang:** Supervision, Writing - review & editing.

Acknowledgments

This research was supported under the National Natural Science Foundation of China (Nos. 21375050 and 21675066), the Research Foundation of Zhenjiang Science and Technology Bureau (No. NY2016011) and the Foundation of Key Laboratory of Sensor Analysis of Tumor Marker, Ministry of Education, Qingdao University of Science and Technology (No. SATM201807).

Supporting information

Materials and apparatus which was used in this work; Figures for optimization of conditions for PEC aptasensor, for determining the conduction band minimum (CBM) and valence band minimum (VBM) of NGQDs and Tauc's plots for Bi_2S_3, tables for comparison of different analytical methods for SDM detection and detection of SDM in milk samples.

Appendix A. Supplementary material

Supplementary data associated with this article can be found in the online version at doi:10.1016/j.bios.2019.01.058.

References

Bai, S., Jiang, J., Zhang, Q., Xiong, Y.J., 2015. Chem. Soc. Rev. 44, 2893–2939.
Białk-Bielińska, A., Maszkowska, J., Mrozik, W., Bielawska, A., Kołodziejska, M., Palavinskas, R., Stepnowski, P., Kumirska, J., 2012. Chemosphere 86, 1059–1065.
Chen, C.C., Ma, W.H., Zhao, J.C., 2010. Chem. Soc. Rev. 39, 4206–4219.
Fang, Z., Liu, Y.F., Fan, Y.T., Ni, Y.H., Wei, X.W., Tang, K.B., Shen, J.M., Chen, Y., 2011. J. Phys. Chem. C 115, 13968–13976.
Gao, M.R., Yu, S.H., Yuan, J.Y., Zhang, W.Y., Antonietti, M., 2016. Angew. Chem. Int. Ed. 55, 12812–12816.
Hong, Y.Z., Jiang, Y.H., Li, C.S., Fan, W.Q., Yan, X., Yan, M., Shi, W.D., 2016. Appl. Catal. B 180, 663–673.
Jiang, D., Du, X.J., Chen, D.Y., Li, Y.Q., Hao, N., Qian, J., Zhong, H., You, T.Y., Wang, K., 2016. Carbon 102, 10–17.
Jiang, D., Du, X.J., Liu, Q., Zhou, L., Dai, L.M., Qian, J., Wang, K., 2015. Analyst 140, 6404–6411.
Jiang, J., Zhao, K., Xiao, X.Y., Zhang, L.Z., 2012. J. Am. Chem. Soc. 134, 4473–4476.
Khezrian, S., Salimi, A., Teymourian, H., Hallaj, R., 2013. Biosens. Bioelectron. 43, 218–225.
Kubacka, A., Fernandez-Garcia, M., Colon, G., 2016. Chem. Rev. 112, 1555–1614.
Li, P., Zhou, Y., Li, H.J., Xu, Q.F., Meng, X.G., Wang, X.Y., Xiao, M., Zou, Z.G., 2015. Chem. Commun. 51 (1743-1743).
Li, R.Z., Liu, Y., Cheng, L., Yang, C.Z., Zhang, J.D., 2014. Anal. Chem. 86, 9372–9375.
Li, Y., Zhao, Y., Cheng, H.H., Hu, Y., Shi, G.Q., Dai, L.M., Qu, L.T., 2012. J. Am. Chem. Soc. 134, 15–18.
Liu, J., Zheng, X., Yan, L., Zhou, L., Tian, G., Yin, W., Wang, L., Liu, Y., Hu, Z., Gu, Z., Chen, C., Zhao, Y., 2015. ACS Nano 9, 696–707.
Liu, Q., Huan, J., Hao, N., Qian, J., Mao, H.P., Wang, K., 2017a. ACS Appl. Mater. Interfaces 9, 18369–18376.
Liu, Q., Huan, J., Hao, N., Qian, J., Mao, H.P., Wang, K., 2017b. ACS Appl. Mater. Interfaces 9, 18369–18376.
Maeda, K., Lu, D.L., Domen, K., 2013. ACS Catal. 3, 1026–1033.
Okoth, O.K., Yan, K., Liu, Y., Zhang, J.D., 2016. Biosens. Bioelectron. 86, 636–642.
Rauf, A., Shah, M.S.A.S., Choi, G.H., Humayoun, U.B., Yoon, D.H., Bae, J.W., Park, J., Kim, W.J., Yoo, P.J., 2015. ACS Sustain. Chem. Eng. 3, 2847–2855.
Sasaki, Y., Kato, H., Kudo, A., 2013. J. Am. Chem. Soc. 135, 5441–5449.
Song, K.M., Jeong, E., Jeon, W., Jo, H., Ban, C., 2012. Biosens. Bioelectron. 33, 113–119.
Wang, X.F., Li, S.F., Ma, Y.Q., Yu, H.G., 2011. J. Phys. Chem. C 115, 14648–14655.
Wetchakun, N., Chaiwichain, S., Inceesungvorn, B., Pingmuang, K., Phanichphant, S., Minett, A.I., Chen, J., 2012. ACS Appl. Mater. Interfaces 4, 3718–3723.
Xia, J.X., Di, J., Li, H.T., Xu, H., Li, H.M., Guo, S.J., 2016. Appl. Catal. B 181, 260–269.
Xu, H., Yan, J., Xu, Y.G., Song, Y.H., Li, H.M., Xia, J.X., Huang, C.J., Wan, H.L., 2013. Appl. Catal. B. 129, 182–193.
Yan, M., Zhu, F.F., Gu, W., Sun, L., Shi, W.D., Hua, Y.Q., 2016. RSC Adv. 6, 61162–61174.
Yang, H.H., Kershaw, S.V., Wang, Y., Gong, X.Z., Kalytchuk, S., Rogach, A.L., Teoh, W.Y., 2013. J. Phys. Chem. C 117, 20406–20414.
Yeh, T.F., Teng, C.Y., Chen, S.J., Teng, H., 2014. Adv. Mater. 26, 3297–3303.
Yin, Y.Y., Liu, Q., Jiang, D., Du, X.J., Qian, J., Mao, H.P., Wang, K., 2016. Carbon 96, 1157–1165.
Yuan, Q.C., Liu, D., Zhang, N., Ye, W., Ju, H.X., Shi, L., Long, R., Zhu, J.F., Xiong, Y.J., 2017. Angew. Chem. Int. Ed. 56, 4206–4210.
Zang, Y., Lei, J.P., Hao, Q., Ju, H.X., 2014. ACS Appl. Mater. Interfaces 6, 15991–15997.
Zhang, Z.J., Wang, W.Z., Wang, L., Sun, S.M., 2012. ACS Appl. Mater. Interfaces 4, 593–597.
Zhao, W.W., Ma, Z.Y., Yu, P.P., Dong, X.Y., Xu, J.J., Chen, H.Y., 2012. Anal. Chem. 84, 917–923.
Zhao, W.W., Xu, J.J., Chen, H.Y., 2014. Chem. Rev. 114, 7421–7441.
Zhao, W.W., Xu, J.J., Chen, H.Y., 2015. Chem. Soc. Rev. 44, 729–741.
Zhao, W.W., Xu, J.J., Chen, H.Y., 2016. TrAC, Trends Anal. Chem. 82, 307–315.
Zhou, P., Yu, J.G., Jaroniec, M., 2014. Adv. Mater. 26, 4920–4935.
Zhu, A., Zhao, Q.D., Li, X.Y., Shi, Y., 2014. ACS Appl. Mater. Interfaces 6, 671–679.
Zhu, M.Y., Liu, Q., Chen, W., Yin, Y.Y., Ge, L., Li, H.N., Wang, K., 2017. ACS Appl. Mater. Interfaces 9, 38832–38841.